UDC 620.17:624.074.1:624.012.45:519.61
Original scientific paper
Received: 02.09.2012.

Experimental study and numerical simulation of the behaviour of concrete dapped-end beams

J. Yolanda Moreno and **Roberto Meli**

Instituto de Ingeniería, Universidad Nacional Autónoma de México, Circuito Escolar,
Ciudad Universitaria, 04510 Mexico City, MEXICO
e-mail: JMorenoM@iingen.unam.mx

SUMMARY

One of the commonly used advantages in the construction of bridges is the possibility of dividing beams into two prefabricated sections imposing thus a hinge without significantly altering the distribution of internal forces with respect to that of a continuous beam. However, a weakness of this solution is the possibility of premature cracking in the re-entrant corner of the dapped-end beam, which may in turn lead to the infiltration of water. For the purpose of this study, three scaled specimens were built and subjected to service load. The first specimen was reinforced according to the guidelines given in PCI design Handbook [1], a longitudinal post-tension was applied to the second one while diagonal bars were placed in the third specimen. The obtained results allow the conclusion that the post-tensioned specimen had a better behaviour, i.e. the post-tensioning is positively correlated with the reduction of cracking. Three-dimensional nonlinear finite element models were created to simulate the cracking of concrete under service load. To this end, smeared crack and discrete crack approach were adopted. The values for cracking obtained by the numerical models showed satisfactory agreement with the experimental tests. It was concluded that in case the necessary parameters for simulation of cracks are obtained from experimental tests, the discrete crack model can be applied to the study of local fracture in reinforced or prestressed concrete structures.

***Key words**: concrete dapped-end beams, discrete crack, smeared crack, cohesive zone model, finite element analysis, post-tension.*

1. INTRODUCTION

The cracking of reinforced and prestressed concrete structures has been researched from both experimental and numerical viewpoints since local failures may occur even under service conditions. This phenomenon has caused concern in the field of civil engineering in which weaknesses in these structures have been recognized when are subjected to high stresses of complex configuration due to sudden changes in its geometry, application of point loads, internal forces at joints with other elements, to name just a few. Dapped-end concrete beams are a representative example of a behaviour that exhibits complex stress states making these structures even more vulnerable to cracking caused by bending-shear interaction.

In literature, the principal failure modes have been identified and design procedures developed to achieve an adequate safety against failure, as exemplified by Mattock and Chan [2], Khan [3], and using strut-and-tie by Barton [4], Mader [5] and Wen-Yao Lu et al. [6]. However, these procedures do not include the review of the diagonal tension in the re-entrant corner, a position where a premature cracking under service load can occur and result in water penetration leading to a progressive degradation by corrosion of the steel. Moreover, the difficulty of visual access to these zones makes it complicated to detect the damage and take timely corrective actions. The prototype of the dapped-end beams taken for this study corresponds to the type of beams used in the constructive system for the bridges recently built in Mexico City (Figure 1).

Fig. 1 Constructive system for bridges recently built in Mexico City

Previous researches have clearly demonstrated that it is possible to analyse the cracking in concrete structures using Finite Element Method (FEM). Two main approaches are typical in this type of analysis: smeared crack approach and discrete crack approach.

A finite element procedure for modelling the non-linear earthquake response of concrete gravity dam systems was presented by Pal [7], Norman [8] and El-Aidi and Hall [9]. In the procedure smeared crack approach was used for tensile cracking. Skrikerud and Bachmann [10] developed a discrete crack procedure to account for the initiation, extension, closure and reopening of tensile cracks. They analysed Koyna Dam which experienced a substantial cracking during the 1967 Koyna earthquake.

2. OBJECTIVES AND SCOPES OF THE RESEARCH

Apart from the numerical modelling procedure, the research programme included an experimental study as well. The experimental section comprised of three tests of specimens of dapped-end beams at scale *1:3.6* with different configurations of reinforcement under service and design load. This paper shows only the results of the application of the symmetrical service load. In each dapped-end beam the associated vertical static load at initial cracking in the re-entrant corner, crack width and crack propagation were provided.

Three-dimensional analysis was performed using the commercial software ANSYS *v.11.0* [11], which employes the FE Method. Three numerical models corresponding to the three specimens tested in the laboratory were created whose simulation involves the application of symmetrical service load.

Finally, the research aims to:

- compare the behaviour of the three types of reinforcement used in the experimental tests under service load;
- obtain the value of the associated load at the initial cracking due to a diagonal tension in the re-entrant corner according to the different reinforcements, as well as its width and propagation; and
- establish an FE Model capable of reproducing the cracking by employing the smeared crack and the discrete crack approach.

3. EXPERIMENTAL TESTS

The behaviour of three dapped-end beams was tested by varying different reinforcements. The zone of interest was recreated, it consisted of a dapped-end of a box beam anchored in slab floor. The application of a vertical, static load directly on the dapped-end by means of two jacks with each having a capacity of *980 kN* was performed in the test. The load was transmitted through a contact plate on the dapped-end of *150×200×24.5 mm* dimensions. A hinged support was placed over the contact plate which transmitted the axial load of the jacks. A load cell was located over each jack. The cell reacted on a loading frame which was anchored in the reaction slab of the laboratory by *6* steel bars, as shown in Figure 2. The bars were tensioned to *294 kN* to ensure a proper support of the specimen on the slab. The specimens were constructed and equipped with instruments in the laboratory of Structures and Materials of Engineering Institute of UNAM. The service load for the dapped-end beams was *177 kN* and was applied symmetrically.

Fig. 2 System of load application

3.1 Description of instrumentation

As a part of the instrumentation, strain gauges were bonded to the steel bars to obtain the strains in order to detect the yield of steel. The strain gauges were placed on the steel grill (main dapped-end reinforcement), hanger reinforcement, upper and lower flexural reinforcement and longitudinal post-tension (Figure 3(a)). Figure 3(b) shows the external instrumentation in which 10 transducers (DCDT) were used. The measurements of these instruments were sent to a Transducer Displacement System (TDS) which converts voltage signals into forces, displacements and deformations. Two micrometers were also placed at the end of the specimen to record the maximum displacement. Finally, a system based on Light Emitting Diodes (LEDs) was placed at 20 points to take the position in space (*x, y, z*) of each LED, at each instant of time by an optical measurement with a high resolution camera (Krypton camera). The crack widths were obtained using this system.

3.2 Description of specimens

The details of specimens are shown in Figure 3.

Specimen E1: Corresponds to the dapped-end beam with a typical reinforcement based on vertical and horizontal hoops and stirrups.

Specimen E2: Besides the mentioned reinforcement, a longitudinal post-tension of *74%* was applied to compress the critical section (re-entrant corner). The longitudinal post-tension was provided by four wires of ϕ *5/8"*, the ultimate stress, f_{pu}, was *1862 MPa*. The tension of each wire was *147 kN*.

Specimen E3: Parts of hanger and grill reinforcements were replaced by diagonal bars at *45°* with the assumption that the diagonal bars, which approximately follow the principal tension, should be more efficient in controlling the cracks in the re-entrant corner.

The specimens were cross-sectional beams of *1000 mm×480 mm*, *1750 mm* long; with the nib having a length of *275 mm* and an overall depth of *250 mm*; typical geometry details are shown in Figure 4(a). Specimen E3 had a change in its geometry owing to the inclusion of an inclination of *50×50 mm* as shown in Figure 4(b). The details of a typical reinforcement are shown in Figure 5, whereas Table 1 provides details of reinforcement modifications.

Table 1. Reinforcement of three specimens by support

Specimen	*No. grill bars*	*No. hangers*	*No. diagonals*	*Post-tension*
E1	*6 - #6*	*8 - #2.5*		
E2	*2 - #4*	*8 - #2.5*		*74%*
E3	*4 - #6*	*4 - #2.5*	*3 - #5*	

Fig. 3 Instrumentation of steel bars and external instrumentation: (a) placement of strain gauges; and (b) placement of potentiometers

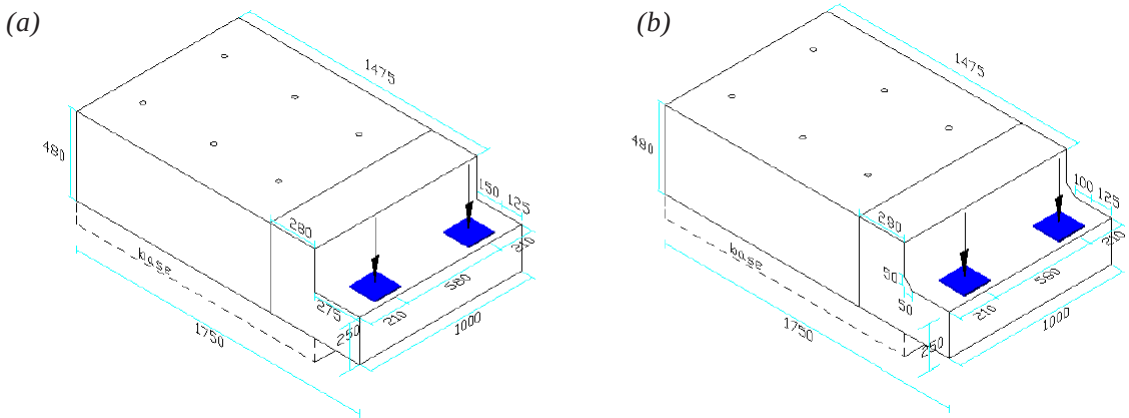

Fig. 4 Geometry of the specimens (units in millimeters): (a) specimens E1 and E2; and (b) specimen E3

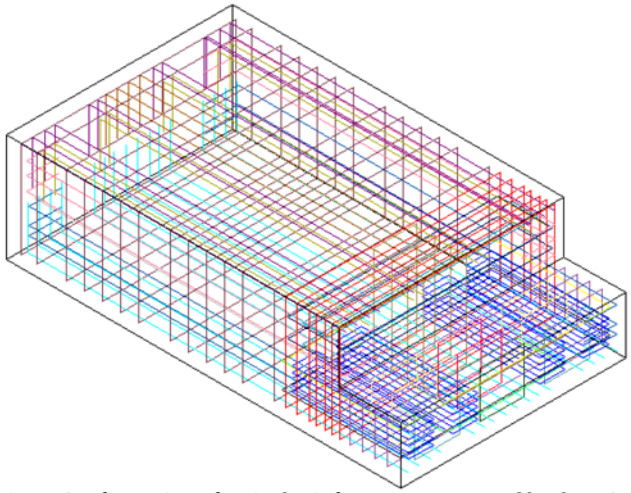

Fig. 5 Configuration of typical reinforcement proposed by the PCI

The reinforcements of each specimen are listed in Table 1, while the configuration of reinforcement and post-tension are illustrated in Figure 6.

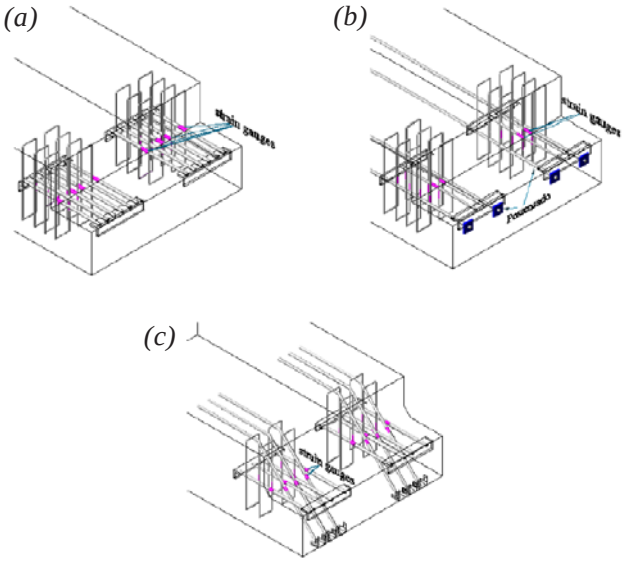

Fig. 6 Configuration of reinforcement and instrumentation of specimens: (a) specimen E1; (b) specimen E2; and (c) specimen E3

The mechanical properties of the materials, compressive strength of concrete, f'_c, tensile strength of concrete, f_t, Young's modulus of concrete, E_c, Young's modulus of steel, f_y, and Poisson ratio, ν, are given in Table 2.

Table 2 Mechanical properties of materials

Material	Specimens	F'_c (MPa)	f_t (MPa)	E_c (Gpa)	f_y (Gpa)	E_s (Gpa)	ν
Concrete	E1 and E2	57.5	4.5	28.2			0.23
	E3	56.4	3.4	27.9			0.22
Hanger bars	E1,E2,E3				408	151	
Grill bars	E1				376	149	
	E2				383	130	0.30
	E3				376	149	
Diagonal bars	E3				394	162	

For each specimen the strength was calculated according to the design equations proposed in section 4.6.3 of the PCI Design Handbook [1]. Equations are based on Mattock's and Chan's proposal [2] and these are appropriate for cases when $a / d \leq 1$, where a is the shear span and d is the depth of the dapped-end beam. The strengths for principal failure modes are shown in Table 3.

The dapped-ends are designed to resist tensile, compressive and shear forces and not to exceed limit states. In the specimens, stresses were principally concentrated in the re-entrant corner causing a diagonal crack starting at the corner.

Table 3. Strength in kiloNewtons of three specimens

Specimen	1	2	3
Yield strength of hangers	402	402	414
Direct shear strength	637	637	637
Flexural strength of dapped-end beam	951	814	877
Diagonal tension shear	1039	1039	1039

3.3 Experimental results

The behaviour of each of the proposed types of reinforcements can be observed from the varying values of the load-displacement curves belonging to the three specimens shown in Figure 7(a). In the phase of the symmetric service load application, specimen E1 had a maximum vertical displacement of *1.01 mm*, and values for specimens E2 and E3 were *0.81 mm* and *0.80 mm*, respectively. The first cracking was observed in the re-entrant corner, (Figure 7(b)) under the following loads: specimen E1 at *88 kN* with a crack width of *0.050 mm*; specimen E2 at *177 kN* with a crack width of *0.040 mm*; and finally, specimen E3 at 118 kN with a crack width of *0.040 mm*. Once the load application was done, the crack widths were *0.065 mm*, *0.040 mm* and *0.045 mm*, for specimens E1, E2 and E3 respectively. The three specimens under the service load had crack widths of less than *0.1 mm*, a usually acceptable value even for the elements exposed to aggressive environments. The specimens E2 and E3 in general exhibited similar stiffness, while specimen E1, after the application of a load of *82 kN* showed a lower stiffness than the others two specimens.

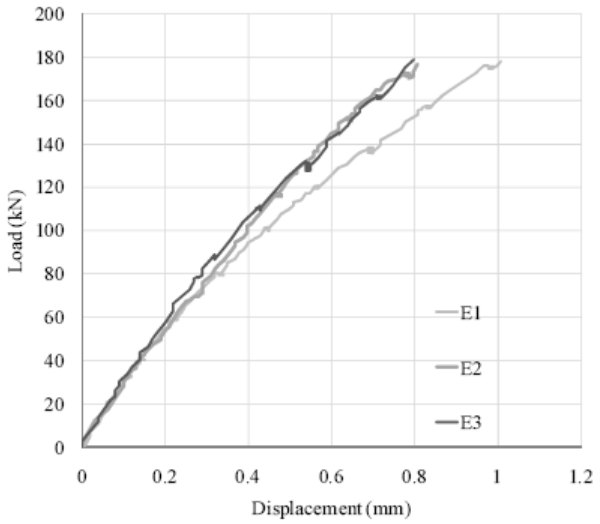

Fig. 7 (a) Load-displacement relationships


Cracking of specimen E1


Cracking of specimen E2


Cracking of specimen E3

Fig. 7 (b) Cracking of three specimens

Specimen E2 generally displayed better behaviour due to deflection under service load, crack width and crack length had smaller values than in the case of the other two specimens. Moreover, the crack closes almost completely once the load is removed, which presents yet another advantage of this type of reinforcement. This behaviour is ascribed to the longitudinal post-tension applied to the beam.

4. NONLINEAR FE ANALYSES

4.1 FE models

The models of the dapped-end beams with three different types of reinforcements were three-dimensional and were created in the software package ANSYS v 11.0 [11]. The cracking was numerically simulated by using the smeared crack approach and the discrete crack approach. Concrete was modelled by using 8-node solid elements. These elements are suitable for the prediction of non-linear behaviour of concrete materials [12] and are suited to model reinforcement with the smeared approach as well. However, a part of reinforcement was modelled using link elements. Discrete crack in the re-entrant corner in the concrete was modelled using the cohesive zone model for the simulation of the delamination process. A perfect bond between rebar and concrete was assumed.

4.1.1 Cracks opening in concrete

The developed cracks in concrete were modelled by contact elements of zero thickness with the crack length of each specimen. The Cohesive Zone Material model (CZM) was defined to activate the delamination of the associated material (interface delamination of contact elements is referred to as *debonding*). Contact analysis was defined surface-to-surface with the CONTA173 element. On the basis of the current mean stress of underlying elements (pair based), the contact stiffness update was obtained in each direction. The behaviour of contact surface was bonded (initial contact).

4.1.2 Discrete crack model

To model a bilinear material behaviour with tractions and separation distances for CZM model the following material constants were used: σ_{max} is the maximum normal contact stress, U_n^c is the contact gap at the completion of debonding, and τ_{max} is the maximum equivalent tangential contact stress.

4.2 Material modelling

4.2.1 Concrete

SOLID65 is the only element in ANSYS capable of modelling the cracking in tension and crushing in compression. It is defined by eight nodes having three degrees of freedom at each node: translations in the nodal *x*, *y*, and *z* directions. Drucker-Prager pressure-dependent failure criterion was applied to the compressive failure of concrete. After crushing, the concrete was assumed to have lost its stiffness in all directions, whereas after cracking, it was assumed to be orthotropic having stiffness based on a linear softening stress-strain response in the normal direction of the crack. The shear transfer coefficients in opening, β_t, or closing β_c, were assumed to take a value of *0.2* and *0.7* respectively.

4.2.2 Steel

Hangers, grills, diagonal bars, and longitudinal post-tension were modelled using LINK8 elements and multilinear isotropic hardening plasticity. The rest of the reinforcement was introduced with smeared approach.

4.2.3 Springs

The bars placed inside the box of the beam and subjected to service load were modelled using COMBIN14 elements introducing the stiffness of each bar. The longitudinal spring-damper is a uniaxial tension-compression element with up to three degrees of freedom at each node: translations in the nodal *x*, *y*, and *z* directions.

4.2.4 Solution method

In the analysis, the service load applied to a model is divided into a series of load increments called load steps using ANSYS Parametric Design Language (APDL). The program uses Newton-Raphson equilibrium iterations for updating the model stiffness. Newton-Raphson equilibrium iterations provide convergence at the end of each load increment within tolerance limits.

4.3 Boundary conditions

Displacement boundary conditions of the model are shown in Figures 8(a) and 8(b). On the basis of the model, the centerline of the beam was constrained (*UX=0*) and at *555 mm* of the nib (*UY=0*). The centerline of the cross-section of the beam was constrained (*UZ=0*) as well. On the box of the beam, elastic springs of zero length were placed to simulate six anchorage bars. The length of the bars was *1430 mm*, having elastic modulus (E_s) of *206 GPa*, and an area (*A*) of *507 mm*^{2}. Inside the specimen, *36*, *24*, and *24* springs were placed as illustrated in Figure 8(b). The stiffness of each bar was divided between the placed springs. On the other hand, the numerical model was displacement controlled through the areas of the plates placed in the experimental tests.

The FE model for the dapped-end beam is shown in Figure 9, while Figure 9(b) illustrates in detail the elements of which the model is considered.

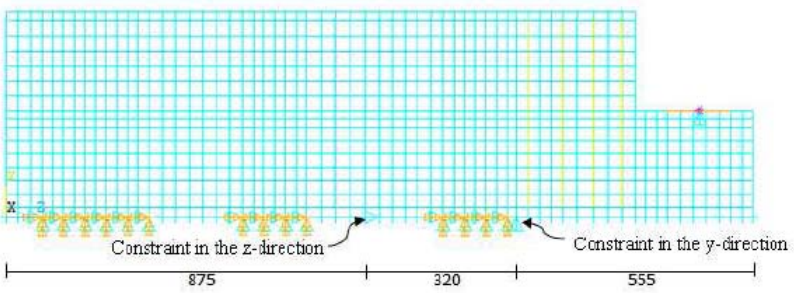

(a)

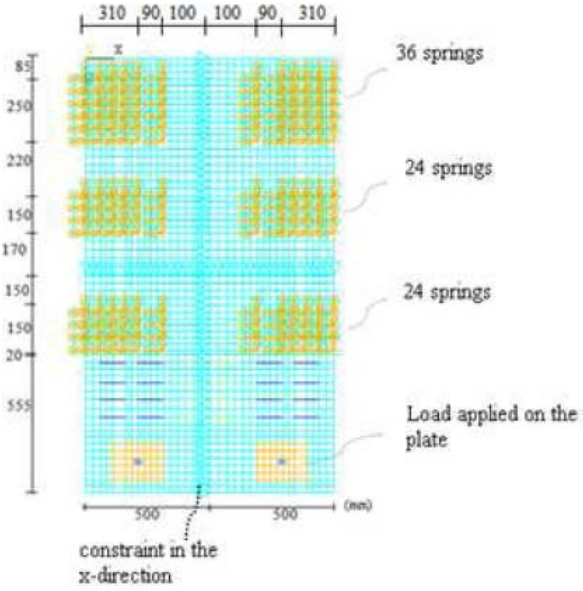

(b)

Fig. 8 Boundary conditions: (a) lateral view; and (b) plan view

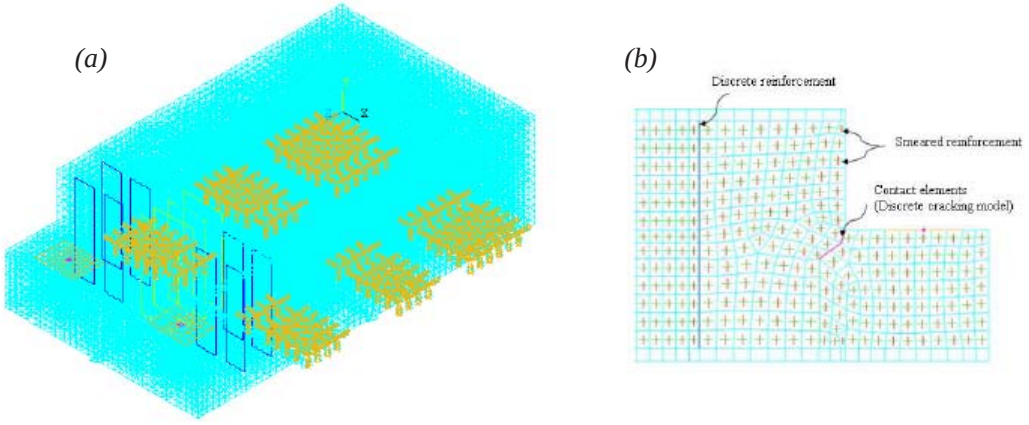

Fig. 9 FE analysis model: (a) isometric view; and (b) details of FE model

5. RESULTS AND DISCUSSIONS

A good correlation between the experimental and numerical results depends on the assignment of accurate linear and non-linear material properties measured experimentally by means of standard tests. Numerical models were called as follows: M1, M2 and M3; corresponding to the numerical simulations of specimens E1, E2 and E3, respectively.

Non-linear properties considered in this paper are shown in Table 4. Cohesion (c), the angle of internal friction (ϕ) and the dilatancy angle (ψ) were taken into account for both models (smeared and discrete). Values of σ_{max}, U_n^c and τ_{max} were considered in the discrete approach based numerical solution for CZM.

Table 4. Nonlinear properties of material

Models	c *(MPa)*	ϕ (°)	ψ (°)	σ_{max} *(Mpa)*	U_c^n *(mm)*	τ_{max} *(Mpa)*
M1	*23.02*	*11.54*	*11.54*	*4.39*	*0.12*	*2.19*
M2	*23.02*	*11.54*	*11.54*	*4.39*	*0.04*	*2.19*
M3	*22.58*	*11.54*	*11.54*	*3.32*	*0.072*	*1.66*

5.1 Load-displacement relationships

Model M1 using smeared crack approach had correlate closely with the experimental curve as shown in Figure 10(a), however the model that used discrete crack approach showed different initial stiffness. This loss of stiffness was a consequence of incorrect simulation in the orientation of the crack. In Figure 10(b), the corresponding models for the simulation of specimen E2 had similar stiffness with the experimental curve until *46 kN* and the value of experimental/numerical relation for displacements under service load was *1.17*. In Figure 10(c) the numerical curves had similar stiffness with the experimental curve until *50 kN* and the value of experimental/numerical relation for displacements under service load was *0.84*.

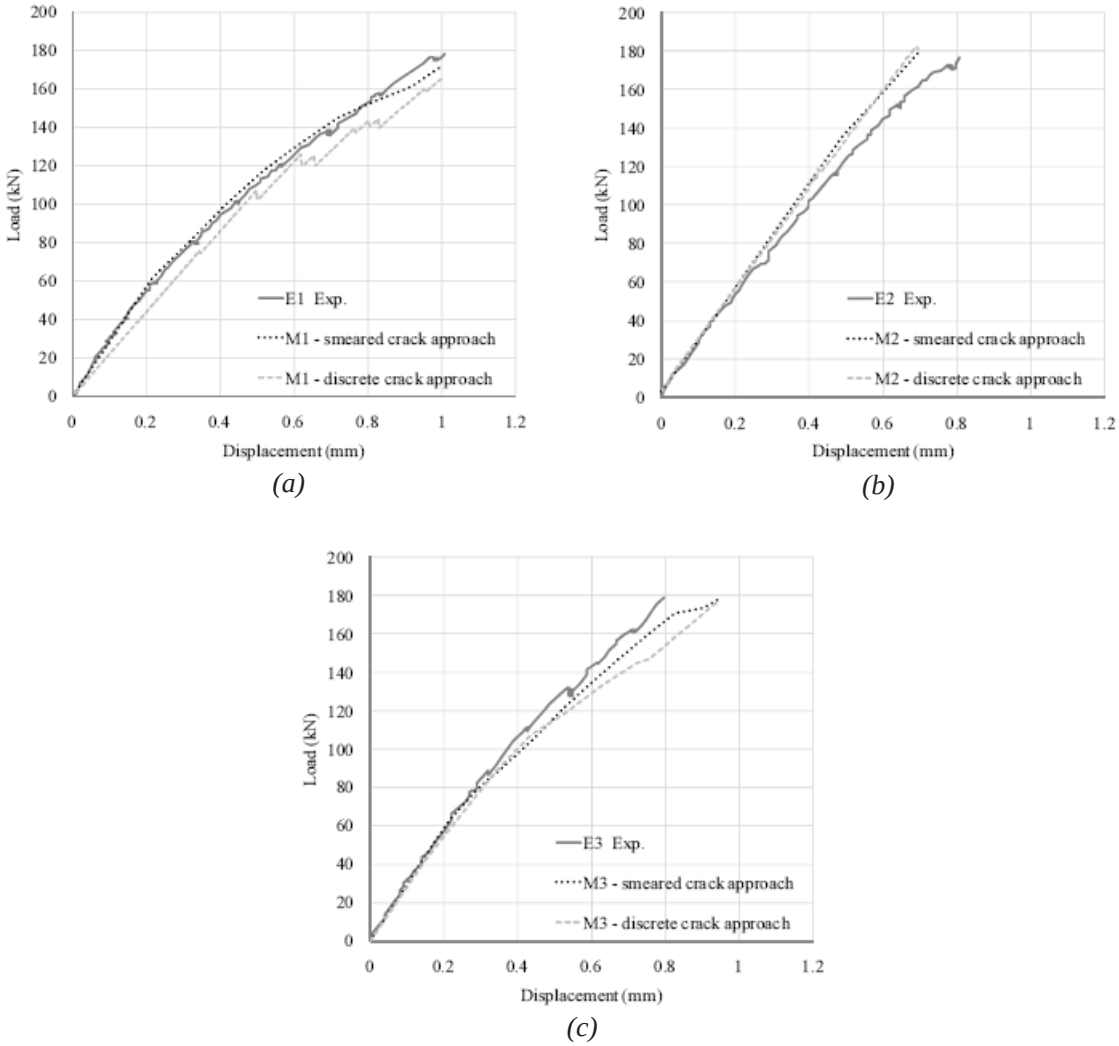

Fig. 10 Load-displacement curves comparison between experimental tests and numerical simulations: (a) models of specimen E1; (b) models of specimen E2; and (c) models of specimen E3

5.2 Cracking under service load

5.2.1 Smeared cracking

Initial cracking was presented in the re-entrant corner as happened in the experimental test. In Figure 11, the initial and final cracking under service load are shown. Initial crack for the model M1 is presented in Figure 11(a) and the final cracking is illustrated in Figure 11(b). For the model M2, the cracking occured at a force of *177 kN*. Finally, the initial and final cracking of model M3 are shown in Figure 11(d) and Figure 11(e) respectively. The initial cracking of the experimental test and numerical simulation for the three dapped-end beams is shown in Table 5.

Table 5. Data of initial cracking

Models	*Initial experimental load (kN)*	*Smeared crack approach (kN)*
M1	*88*	*81*
M2	*177*	*177*
M3	*118*	*80*

5.2.2 Discrete cracking

It is complicated to define crack orientation in numerical simulation using the discrete crack approach since in the experiment the crack of the specimens E1 and E3 changed their orientation during the propagation. Therefore, in the model an equivalent crack was simulated instead. This assumption affected the obtaining of the load-displacement curve (Figure 10) and crack widths (Table 6). Debonding for normal separation (Mode I) was the condition that the cracks followed in the three models.

Discrete cracking and stress map "Z" are shown in Figure 12; the models also provided the smeared cracking due to concrete element being used. In Figures 12(b), 12(d) and 12(f) it is possible to note the opening of the diagonal crack. The only model that presented closely tension to concrete strength was model M1.

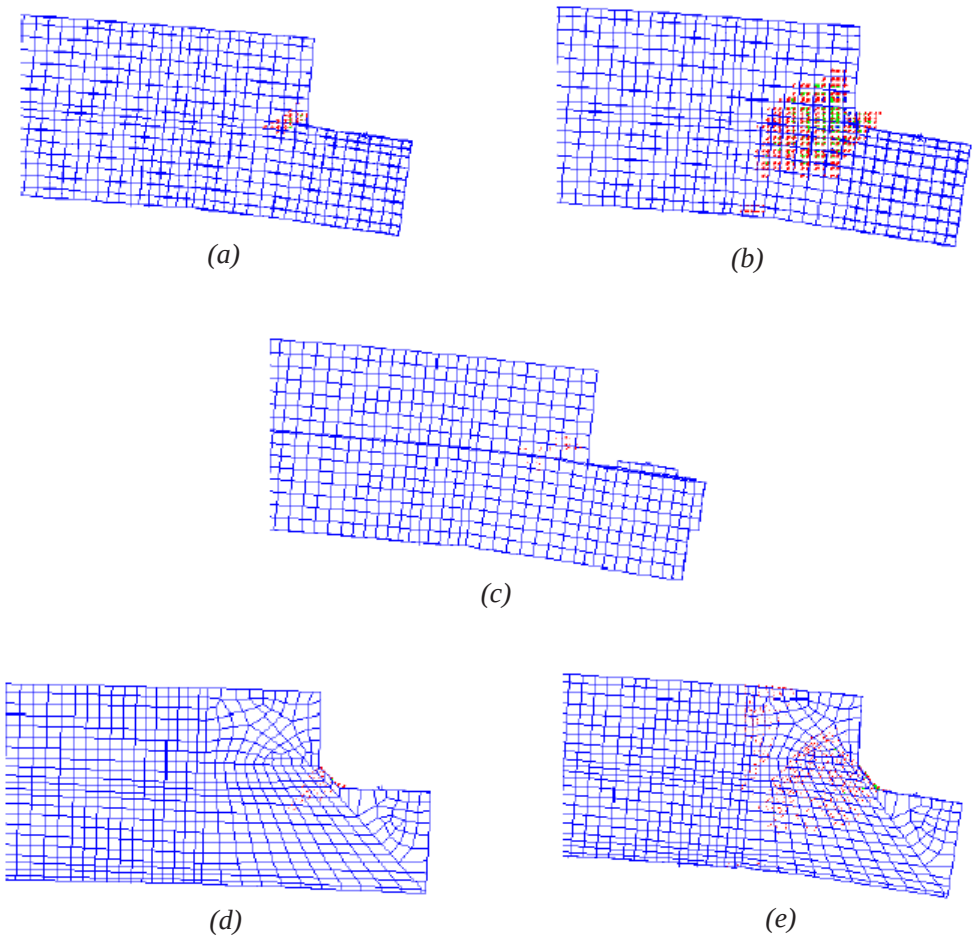

Fig. 11 Development of cracking under symmetric service load (smeared crack approach): (a) initial cracking of model M1; (b) final cracking of model M1; (c) cracking of model M2; (d) initial cracking of model M3; and (e) final cracking of model M3

Table 6. Crack widths obtained of experimental tests and numerical simulations models load (kN)

Models	*Load (kN)*	*Experimental crack width (mm)*	*Numerical crack width (mm)*
M1	*88*	*0.050*	*0.057*
	118	*0.054*	*0.079*
	176.5	*0.065*	*0.118*
M2	*176.5*	*0.040*	*0.038*
M3	*118*	*0.040*	*0.059*
	137	*0.044*	*0.066*
	176.5	*0.045*	*0.072*

Model M2 exhibited a crack width similar to the experimental crack width, while the cracks belonging to models M1 and M3 correspond to their experimental counterparts only until *88 kN* and *118 kN* respectively. A general conclusion that can be drawn is that the numerical analysis have shown there to be a positive correlation between the expansion of crack widths and the increase of load. Another conclusion to be mentioned is that the induced crack width causes the zones with smeared cracking to decrease.

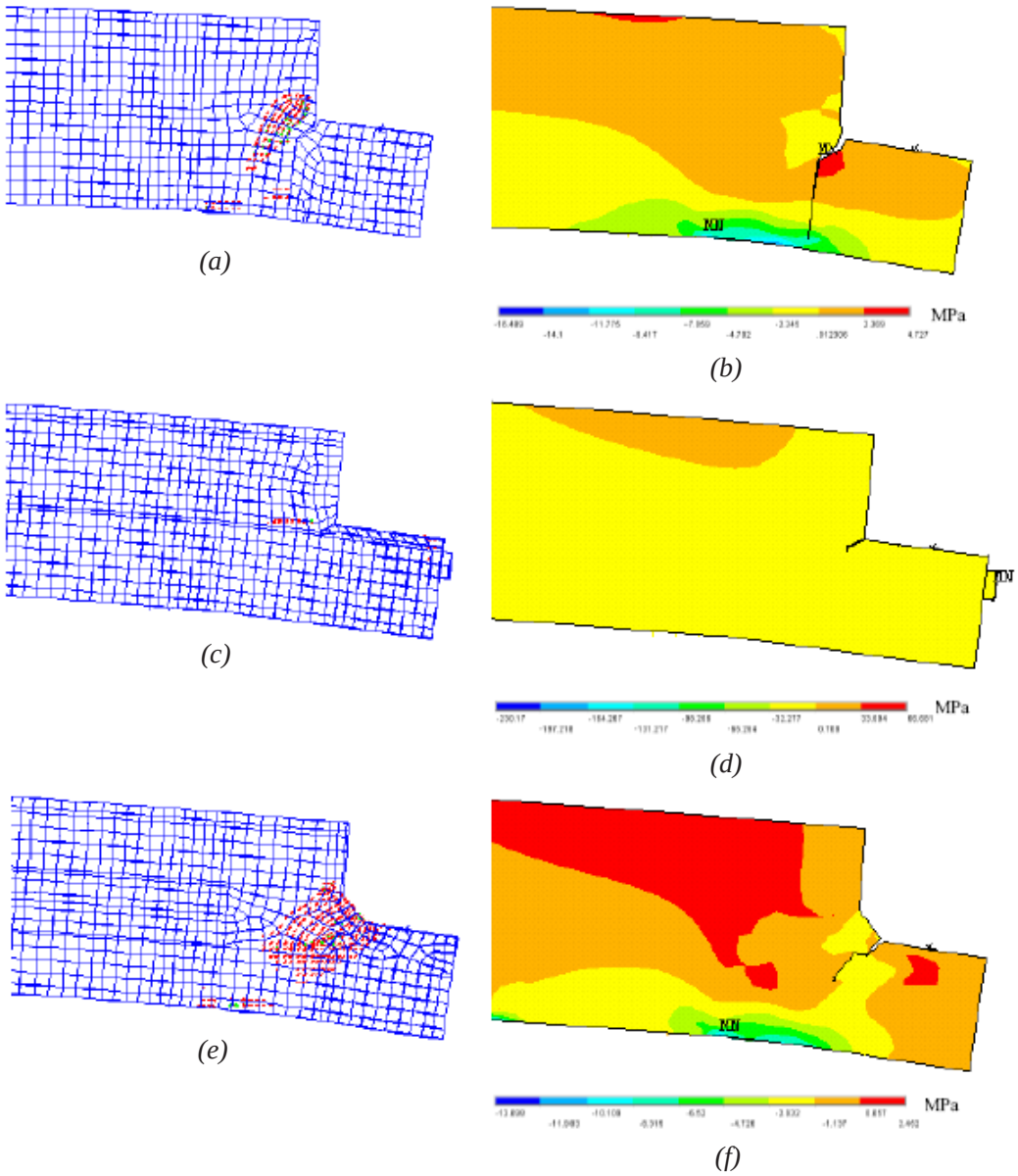

Fig. 12 Development of cracking using discrete crack approach, smeared cracking and stress maps: (a) smeared cracking of model M1; (b) opening of discrete crack of model M1; (c) smeared cracking of model M2; (d) opening of discrete crack of model M2; (e) smeared cracking of model M3; and (f) opening of discrete crack of model M3

6. CONCLUSIONS

In this paper, three concrete dapped-end beams were tested with the purpose of comparing the behaviour of three types of reinforcements under service load. Other objectives are obtaining the values of the associated load at the initial cracking and the crack widths, as well as to observe the development of cracks due to a diagonal tension in the re-entrant corner. Also, a numerical analysis to evaluate the cracking using the smeared crack approach and the discrete crack approach was established. The FE models were compared with the experimental results.

The results obtained from the tested specimens in the laboratory are the following:

- The behaviour of three specimens under service load had crack widths lower than *0.1 mm*, a value usually considered admissible even for elements exposed to aggressive environments.
- The inclined dapped-end (specimen E3) is more efficient compared to the rectangular dapped-end (specimen E1).
- Results allowed to conclude that the post-tensioned specimen generally exhibited a better behaviour owing to its deflection, crack width and crack length that were smaller than in the others two cases. Another advantage of this type of reinforcement is the fact that the crack closes almost completely once the load is removed.

On the basis of the numerical results, the following conclusions were obtained:

- The numerical models predicted almost completely and accurately the associated load at the initial cracking in the re-entrant corner when compared with those obtained in the experimental tests.
- The smeared crack approach is a tool more general for solving the practical problems in engineering, i.e. it showed good correlation between the tests and numerical simulations, while the discrete crack approach is a better option when the crack orientation is known with its parametric values of material.
- Debonding for normal separation (Mode I) was the condition that the cracks followed under service load.
- Model M2 showed a similar crack width to experimental crack width, because the crack only had an orientation.

7. ACKNOWLEDGEMENTS

The first author wishes to express her gratitude to the “Consejo Nacional de Ciencia y Tecnología – CONACYT”, “Instituto de Ingeniería UNAM,” professor Gelacio Juárez for the continuous support of the research and Dr. Marcos Chávez.

8. REFERENCES

[1] *PCI Design Handbook: Design of Precast and Prestressed Concrete Components*, Chapter 4: Design of precast and prestressed concrete components, PCI, Chicago, pp. 79-83, 2004.

[2] A.H. Mattock, K.C. Chen and K. Soongswang, The behaviour of reinforced concrete corbels, *Journal of the Prestressed Concrete Institute*, Vol. 21, No. 2, pp. 52-77, 1976.

[3] M.A. Khan, A study of the behaviour of reinforced concrete dapped-end beams, M.Sc. Thesis, University of Washington, Seattle, pp. 145, 1981.

[4] D.L. Barton, Detailing of structural concrete dapped end beams, M.Sc. Thesis, University of Texas at Austin, Austin, 1988.

[5] J.M. Mader, Detailing dapped ends of pre-tensioned concrete beam, M.Sc. Thesis, University of Texas at Austin, Austin, 1990.

[6] W.-Y. Lu, I.-J. Lin, Sh.-J. Hwang and Y.-H. Lin, Shear strength of high-strength concrete dapped-end beams, *Journal of the Chinese Institute of Engineers*, Vol. 26, No. 5, pp. 671-680, 2003.

[7] N. Pal, Seismic cracking of concrete gravity dams, *ASCE Journal of the Structural Division*, Vol. 102, No. ST9, pp. 1827-1844, 1976.

[8] C.D. Norman and F.A. Anderson, Reanalysis of cracking in large concrete dams in the U.S. Army Corps of Engineers, Proc. 15th Int. Conf. on Large Dams, Question 57 (9), pp. 157-171, Lausanne, 1985.

[9] B. El-Aidi and J.F. Hall, Non-linear earthquake response of concrete gravity dams - Part 1: Modelling, *Earthquake Engineering and Structural Dynamics*, Vol. 18, No. 6, pp. 837-851, 1989.

[10] P.E. Skrikerud and H. Bachmann, Discrete crack modelling for dynamically loaded unreinforced concrete structures, *Earthquake Engineering and Structural Dynamics*, Vol. 14, No. 2, pp. 297-315, 1986.

[11] ANSYS, Documentation for ANSYS, ANSYS Workbench Release 11.0 Environment, ANSYS Inc., 2006.

[12] K.J. William and E.P. Warnke, Constitutive model for the triaxial behaviour of concrete, IABSE Report, Vol. 19, Proc. of the IABSE Colloquium on Concrete Structures Subjected to Triaxial Stresses, ISMES, Bergamo, pp. 1-30, 1974.

EKSPERIMENALNA ISTRAŽIVANJA I NUMERIČKA SIMULACIJA PONAŠANJA BETONSKIH GREDA S KONZOLNIM ZAVRŠETKOM

SAŽETAK

Jedna od prednosti koje se koriste pri projektiranju mostova je mogućnost podjele betonskih greda u dva montažna dijela pritom stvarajući zglob na poziciji spoja te time ne mijenjajući značajnije raspodjelu unutarnjih sila u odnosu na raspodjelu koja se javlja u kontinuiranoj gredi. Međutim, nedostatak ovakvog rješenja leži u mogućnosti prijevremenog pucanja konzolnog dijela (re-entrant corner) grede s konzolnim završetkom (dapped-end beam), što posljedično može dovesti do prodora vode u betonsku konstrukciju. Tri uzorka izrađena su u smanjenom mjerilu te su podvrgnuta uporabnom opterećenju. Prvi uzorak pojačan je prema smjernicama zadanim u PCI priručniku za projektiranje. Na drugome uzorku primijenjeno je longitudinalno, naknadno prednapinjanje, a u treći uzorak su umetnute dijagonalne šipke. Iz rezultata se može zaključiti da uzorak s primijenjenim naknadnim prednapinjanjem pokazuje najbolje ponašanje glede smanjenja pukotina u betonu. Nelinearne, 3D simulacije, modelirane pomoću metode konačnih elemenata provedene su kako bi se prikazalo nastajanje pukotina u gredi pod uporabnim opterećenjem, a pritom su korišteni modeli diskretnih i razmazanih pukotina. Vrijednosti pukotina dobivene numeričkom simulacijom uvelike se poklapaju s vrijednostima dobivenima eksperimentalnom analizom. Naposlijetku, može se zaključiti da je diskretni model pukotine primjenjiv u slučaju lokalnog sloma u klasično armiranim i prednapetim betonskim konstrukcijama ukoliko su parametri za simulaciju pukotina prethodno dobiveni eksperimentalnom analizom.

***Ključne riječi**: betonske grede s konzolnim završetkon, diskretni model pukotine, razmazani model pukotine, model kohezivne zone, numerička analiza primjenom metode konačnih elemenata.*